

# Near-surface Mounted Technology in Strengthening Reinforced Concrete Beam

Muhammad Adam Syahmi Dazulhisham<sup>1</sup>, Muhammad Arif Ikmal Abdul Halim<sup>1</sup>, Lyn Dee Goh<sup>1\*</sup>

<sup>1</sup> Civil Engineering Studies, College of Engineering,  
Universiti Teknologi MARA Cawangan Pulau Pinang, 13500 Permatang Pauh, Pulau Pinang, MALAYSIA

\*Corresponding Author: [gohlyndee147@uitm.edu.my](mailto:gohlyndee147@uitm.edu.my)

DOI: <https://doi.org/10.30880/ijie.2024.15.01.015>

## Article Info

Received: 27 February 2024

Accepted: 25 March 2024

Available online: 15 July 2024

## Keywords

Strengthening, near-surface mounted, elevated temperature, reinforced concrete beam

## Abstract

Structural strengthening is essential in civil engineering to ensure the integrity, safety, and longevity of various types of structures. Effective strengthening is required to solve these issues and lengthen the service life of structures as they naturally deteriorate with time. Hence, the use of various strengthening techniques to enhance the structural integrity of existing structures and infrastructure has gained prominence in recent years. This study demonstrates how Reinforced Concrete (RC) structures may benefit from Near-Surface Mounted (NSM) technology. The demonstration involves the experimental study on the performance of three different types of RC beams; unstrengthened RC beam, RC beam strengthened with NSM procedure using a conventional steel ribbed bar, and RC beam strengthened with NSM procedure using an iron-based smart memory alloy (Fe-SMA) ribbed bar. Consequently, three RC beams were evaluated at room temperature throughout the experimental testing, while the remaining three RC beams were examined after being exposed to a 200°C temperature exposure. The load-deflection, strain deformation and crack propagation were demonstrated to determine the behaviour of the RC beam. The experimental findings suggested that the performance of RC beams strengthened using NSM techniques was superior to that of RC beams that had not been strengthened. Although the results generally indicated a decrease in ultimate load obtained in the RC beams exposed to elevated temperature compared to RC beams tested at room temperature. It is shown that Fe-SMA RC beams performance better compared to steel strengthened RC beams. The RC beams strengthened with an Iron-based smart memory alloy ribbed bar recorded an increase in load-carrying capacity. These results demonstrate the substantial variations in load-bearing capacities among the beams and emphasise the efficiency of the strengthening application for RC beams in the constructions industry, particularly the use of iron-based smart memory alloy ribbed bars as strengthening materials

## 1. Introduction

Reinforced Concrete (RC) structures can experience excessive damage due to overloading, ageing, man-made error during design and execution, and environmental exposure [1]-[3]. As a result, strengthening is frequently recommended in RC constructions to achieve appropriate strength requirements and increase service life.

Repairing or strengthening structures is both environmentally and economically preferable compared to total replacement or demolition.

Over the past decade, extensive research has been conducted on strengthening concrete structures using various methods such as external bonding, jacketing, epoxy strengthening and prestressing methods [4]-[8]. Although this strengthening method offers an increase in the load-carrying capacity of RC structures, each method has its own drawbacks. For instance, the external bonding method involves adhering composite elements to the concrete surface with high-strength epoxy adhesives. In recent years, the preferred composite material commonly used for the external bonding method is Fibre-Reinforced Polymer (FRP). This choice is attributed to FRP's high strength, lightweight, excellent corrosion resistance, and ease of fabrication [9], [10]. However, the most significant weakness of the external bonding approach is early debonding, which can prevent FRP composites from reaching their maximum tensile capability, wasting expensive FRP materials [11], [12]. On the contrary, jacketing involves the addition of an extra layer of material around an existing structural element, such as wrapping the concrete element with a new layer. This additional layer is typically made of RC, FRP composites, or steel plates. Nevertheless, Mahmoud et al. [13] and Karim and Karim [14] identified that the weakness of jacketing is very significant for several reasons. Generally, it is a dirty and disruptive method, increasing in cost of non-structural damage caused by the jacket construction and the architectural problems that the jacketing can impose.

In the context of exploring various existing strengthening methods for concrete structures, it is noteworthy to mention the recent surge in interest and practical applications of the Near-surface Mounted (NSM) technology. This technology enhances RC elements by installing additional reinforcement elements close to the surface of the concrete to provide additional tensile strength to the concrete without affecting the original structure's dimensions. Furthermore, this technology has been garnering attention due to its potential advantages over other approaches, such as reduced site installation work, higher bonding efficiency, and better protection of the strengthening materials. It also fully employs the strength of the materials, as highlighted by De Lorenzis et al. [15], Xing et al. [16], and Zhang et al. [17]. However, challenges arise concerning prestressing capabilities when using the prestressed steel reinforcement in the NSM technology. Although they are widely adopted for their mechanical properties and availability, prestressed steel reinforcement requires careful engineering techniques to achieve the desired prestress force, as reported by Geetha and Selvakumar [18] and Hong et al. [19]. This can lead to potentially increased labour intensity and cost implications, even for small-scale projects. It is worth mentioning that Obaydullah et al. [20] acknowledged that prestressing steel can be a complex and intricate process, even after the initial prestressing is completed. Hence, the need for continued use of hydraulic jacks during the curing period highlights the challenges involved in maintaining the desired prestress levels and preventing relaxation or loss of force in the steel.

Amidst these challenges, Shape Memory Alloy (SMA), particularly Iron-based SMA (Fe-SMA), offer a promising alternative for overcoming the limitations of prestressed steel reinforcement in the NSM technology. The unique properties of Fe-SMA, including super-elasticity and the ability to undergo significant deformation and return to their original shape [2], [21], [22], enable them to be prestressed efficiently within the concrete matrix. This advantage simplifies the strengthening process and ensures more effective utilisation of prestressing, leading to enhanced load-carrying capacity and improved structural performance. Numerous studies on utilising Fe-SMA for strengthening RC beams have been reported in the literature [23]-[25]. However, most of these investigations have primarily focused on different technology, such as external bonded applications and NSM using steel anchorage systems. In contrast, the method proposed in this study utilises a simple and easily obtainable cementitious grout for Fe-SMA ribbed bar. This unique approach offers advantages in terms of cost-effectiveness and ease of implementation, making it a viable option for practical applications. Furthermore, one crucial aspect that sets this study apart from past research is investigating the strengthened structures' performance under elevated temperature conditions. Meanwhile, previous studies have explored SMA strengthening under various loading scenarios. The effect of elevated temperatures on the behaviour and load-carrying capacity of structures strengthened with Fe-SMA has remained relatively unexplored. This study aims to bridge the knowledge gap and provide valuable insights into the feasibility and effectiveness of strengthening RC beams with the NSM method using Fe-SMA rounded ribbed bars. The load-deflection and strain deformation of the strengthened RC beams were investigated. Moreover, a conventional rounded ribbed steel bar is also employed in this study for comparison purposes. Note that the experimental study covers two distinct conditions: the first being at room temperature and the second under elevated temperature conditions.

## 2. Methodology

A total of six (6) RC beams were constructed in this study. Each beam had dimensions of 200 mm in height, 150 mm in width, and 750 mm in length. Table 1 presents the tested specimens of RC beams in this study. The first type, CB1, represented unstrengthened RC beams, while the second type, A1, was strengthened with NSM using conventional steel ribbed bar, and the third type, B1, was strengthened with NSM using Fe-SMA ribbed bar. Both

bars were rounded bars of diameter 10 mm. These beams were initially tested at room temperature using a four-point bending test. Subsequently, a subset of the RC beams (CB2, A2, and B2) was exposed to an elevated temperature of 200°C for two hours before undergoing testing with a similar four-point bending test. The beams' reinforcement configuration is presented in Fig. 1. All tested RC beams were designed according to Eurocode 2: Design of Concrete Structure. Table 2 shows the design parameters used to design the RC specimens. The beams are reinforced with two compression bars with a diameter of 10 mm and two 12 mm diameter tensile bars at the bottom of the beam. Other than that, shear reinforcements in the RC beams comprised 6 mm diameter bars spaced at 100 mm centre to centre.

**Table 1** Details of strengthened beams

Beam ID	Exposure to High Temperature
CB1	Room Temperature
CB2	200°C
A1	Room Temperature
A2	200°C
B1	Room Temperature
B2	200°C

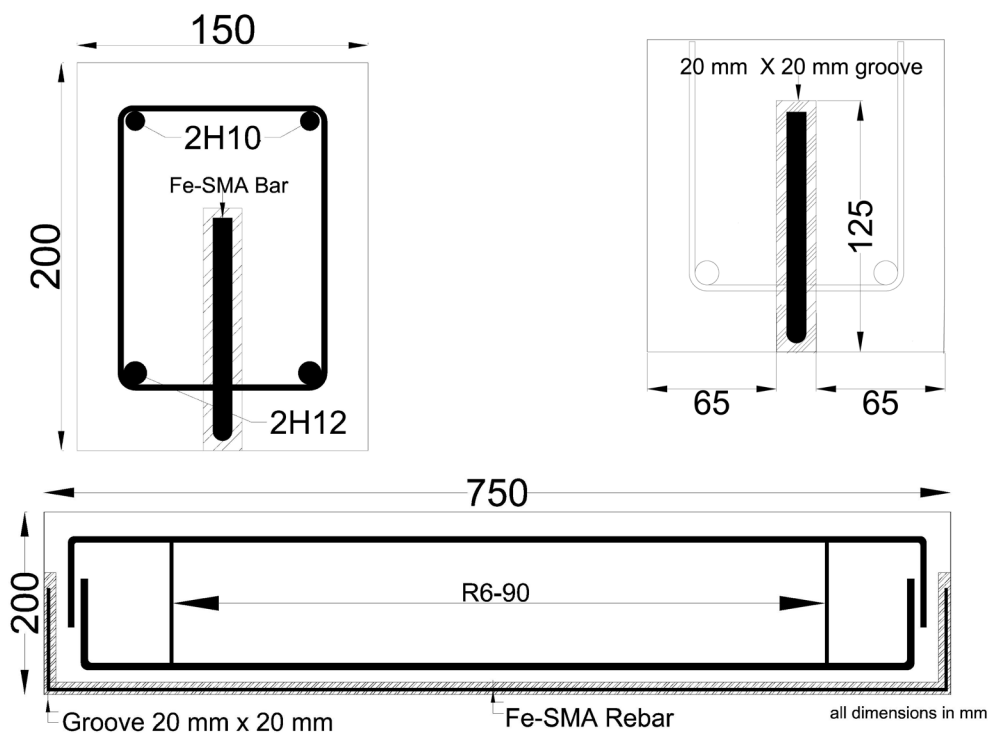


**Fig. 1** Details of RC beams strengthened with Fe-SMA ribbed bar and steel ribbed bar

**Table 2** Design parameters of the RC beam

Design Parameters	
Concrete Compressive Strength	30 MPa
Exposure Class	XC1
Structural Class	S4
Design Fire Resistance	R60
Concrete Cover	40 mm

## 2.1 Materials Properties

### 2.1.1 Concrete and Steel

The compressive strength of the concrete was tested according to EN12390-3, Testing hardened concrete. A total of six (6) cubes were prepared to be tested on day 7 and day 28. At 28 days, the concrete design strength was targeted to be 30 MPa. Compressive strength tests were conducted on the concrete specimens on days 7 and 28 and obtained 33.33 MPa and 39.93 MPa, respectively. As for steel reinforcements, a Universal Tensile Machine (UTM) with 1000 kN capacity was employed to test the tensile strength of the reinforcements. The results of the tensile test are recorded in Table 3. The compression rebar (2H10) recorded a yield stress of 273.4 MPa and ultimate stress of 397.6 MPa, while the tensile reinforcement (2H12) recorded a yield stress of 299.7 MPa and ultimate stress of 419.7 MPa. The shear reinforcement (R6) yield stress and ultimate stress is 259.3 MPa and 402.3 MPa, respectively. As for the cementitious grout, Sika215, the material's compressive strength at 28 days is 60 MPa.

**Table 3** Tensile properties of the steel reinforcements

	H12	H10	R6
Maximum Stress (MPa)	419.683	397.596	402.284
Yield Stress (MPa)	299.704	273.404	259.229

### 2.1.2 Fe-SMA Ribbed Bar Properties

In this study, the Fe-SMA ribbed bar was produced by EMPA & Refer.AG, a Swiss company. The specific composition of the ribbed bar consists of the following elements: 17% iron (Fe), 5% manganese (Mn), 5% silicon (Si), 4% chromium (Cr), 1% nickel (Ni), and 1% combined vanadium and carbon (V, C) content, all measured in terms of mass percentage, Fe-17Mn-5SiCr-4Ni-1(V, C) (mass%). The physical properties of the Fe-SMA are shown in Table 4. The Fe-SMA rebar was prestrained at 4% to induce the shape memory effects (SME). The diameter of the Fe-SMA ribbed bar employed in the study was 10 mm, and its activation temperature was set at 160°C. Similar composition of Fe-SMA and activation temperature were also applied in the study conducted by Czaderski et al. [26]. Note that the ultimate stress of the Fe-SMA ribbed bar is 1051 MPa with an elongation of 30%. Fe-SMA is more suitable for strengthening concrete applications due to its stable transformation hysteresis, lower cost, and high elastic stiffness compared to other SMAs, such as those based on nitinol. When heated, the Fe-SMA attempts to return to its original shape, generating recovery stress. This recovery stress can be harnessed to induce prestressing in the structure, inducing compression in the surrounding concrete. According to Shahverdi et al. [27], the recovery stress induced by the Fe-SMA varied from 315 MPa to 350 MPa, as presented in Fig. 2.

**Table 4** Physical properties of Fe-SMA by Zhang et al., [27]

Property	Value
Density	7.2 g/cm <sup>3</sup>
Young's modulus	170 GPa
Electrical Resistivity	100 μΩ·cm
Specific Heat Capacity	540 J/kg·°C
Thermal Conductivity	8.4 w/(m·°C)
Thermal Expansion Coefficient	16.5 (×10 <sup>-6</sup> ) °C <sup>-1</sup>
Melting Point	1320 °C
Poisson's ratio	0.359

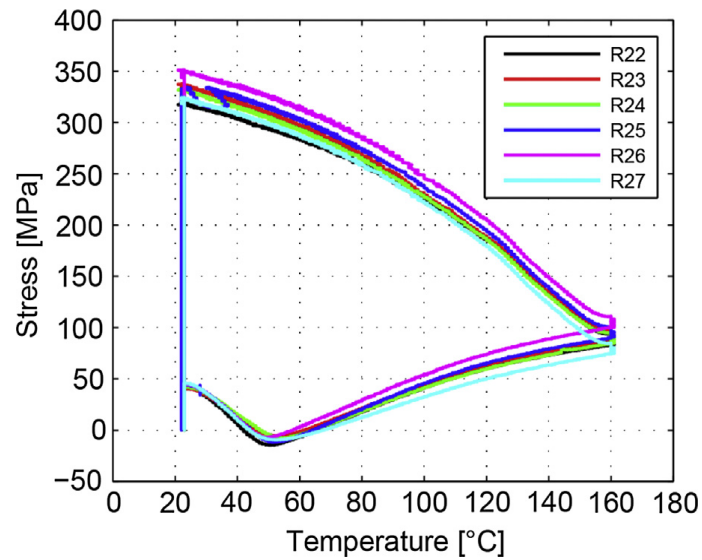


**Fig. 2** Recovery stress results of Fe-SMA bar with 10 mm diameter, Shahverdi et al., [27]

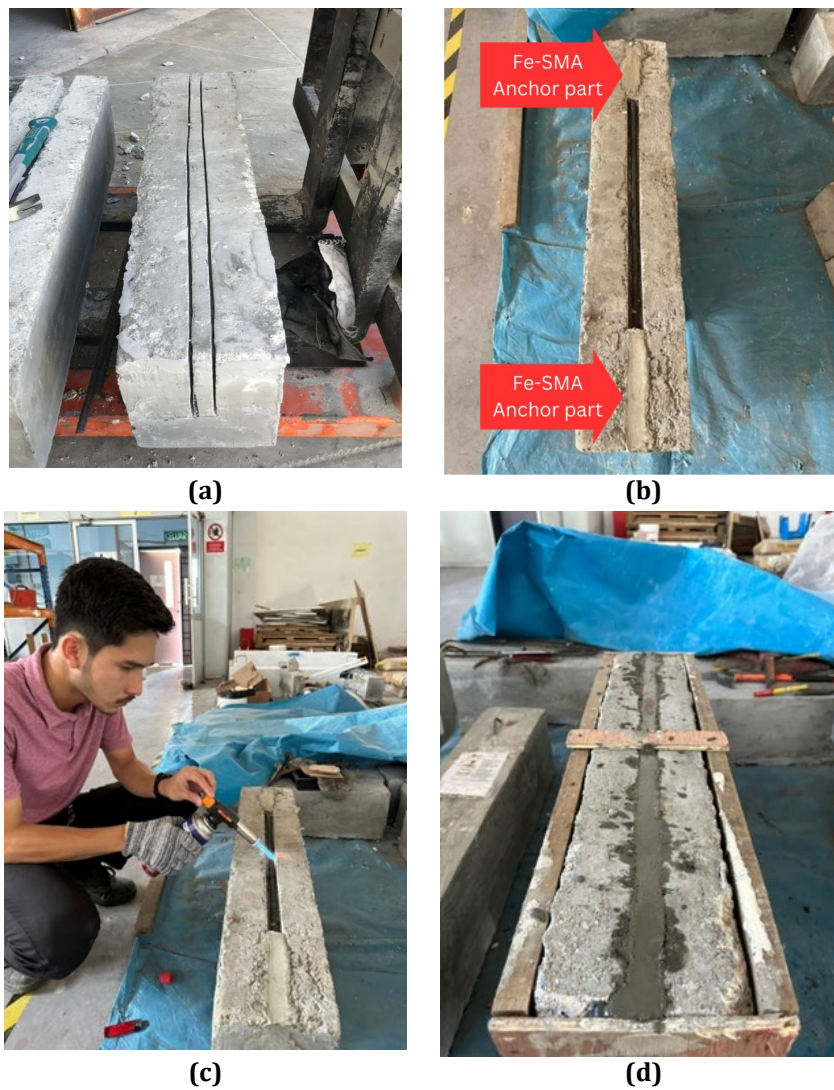


**Fig. 3** The NSM strengthening procedure (a) Groove cutting process using special concrete saw; (b) Restraint of Fe-SMA bars at both ends using Sikagrout215; (c) Heating of SMA bars at 160°C using heat torch; (d) Filling of groove using Sikagrout215

## 2.2 Strengthening Procedure

The NSM strengthening procedure involved using a concrete saw equipped with a diamond blade to create a groove at the soffit of the RC beam specimens. This groove, measuring 20 mm in height, 20 mm in width, and 750 mm in length, starts at the concrete cover in the tension area along the longitudinal direction, as displayed in Fig. 3(a). The groove dimensions were adopted from ACI 440.2R-17. Furthermore, the groove was extended vertically upward for 125 mm on each side while maintaining the same width and depth. This extended groove aimed to create sufficient anchorage length of the Fe-SMA ribbed bar in the concrete. A hammer and a hand chisel were employed to remove any remaining concrete lugs and roughen the groove's surface. For specimens with conventional steel ribbed bars, the ribbed bar was placed into the grooves and then filled with cementitious grout, Sika215 completely. The mixing ratio of these cementitious materials used was 1.84 kg Sika215 mixed with 0.31 L water, which produced 1 liter of cementitious grout. Meanwhile, the Fe-SMA ribbed bar was placed into grooves cut as presented in Fig. 3(b) and was anchored at both ends using cementitious grout, Sika215. Subsequently, the Fe-SMA ribbed bar was heated at 160°C using a heat torch, as illustrated in Fig. 3(c), to activate the shape memory effect of the SMA ribbed bar. This produces a recovery stress that acts as prestressing for the RC beams. An infrared temperature gun was used to monitor the temperature changes, avoiding the Fe-SMA from overheating. Excessive heat of the Fe-SMA can reduce recovery stress. The groove was then filled with Sikagrout 215, as portrayed in Fig. 3(d), to complete the NSM procedures at let for cured for at least 28 days.

## 2.3 Exposure to Elevated Temperatures

After the strengthening procedure was completed, the three (3) RC beam specimens tested under elevated temperature of 200°C were placed in the electric furnace for temperature exposure for two hours. Subsequently, all specimens were allowed to be cooled at room temperature before testing the RC beams. Fig. 4 shows the elevated temperature curve used in this study.

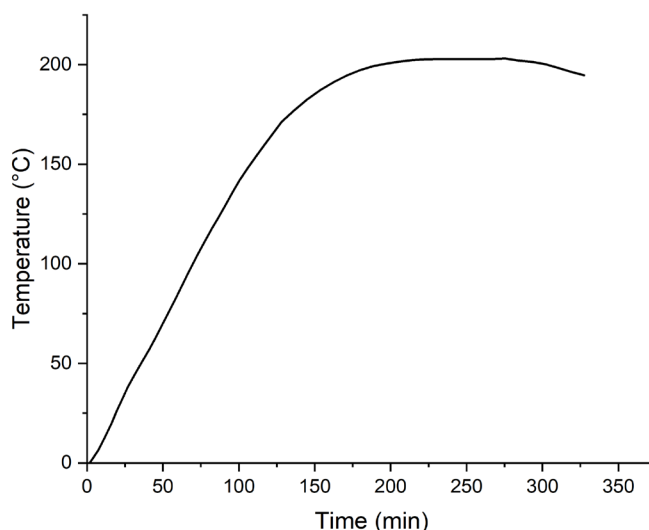


Fig. 4 Elevated temperature curve of 200°C

## 2.4 Test Setup

Four-point flexural tests were performed to investigate the behaviour of the RC beams in accordance with BS EN 12390-5:2009, as displayed in Fig. 5. The RC beams were simply supported with a net length of 650 mm, and the two loading points were 215 mm. A hydraulic jack with a capacity of 250 kN, and a load cell with the same capacities were used. The load was applied at 5 kN per level, and during the intervals, the cracks propagation were recorded. Three Linear Variable Differential Transformers (LVDT) were mounted at the beam soffit to record the vertical displacements. In contrast, four (4) strain gauges were installed; two at the RC beam's maximum tensile layer and two at the maximum compression of the RC beams to record the RC beams strain.

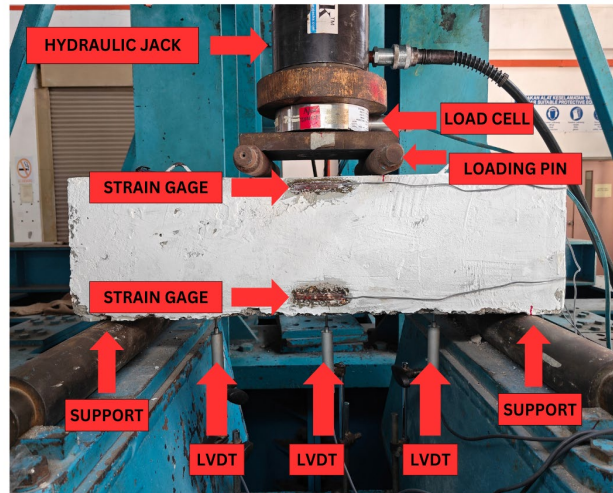


Fig. 5 Test setup in the laboratory

### 3. Results

#### 3.1 Initial Crack Load

##### 3.1.1 Room Temperature

The initial crack of the RC beam is one of the critical points that indicates the structural behaviour of the RC beams. RC beam is strong in compression but weak in tension. This caused the bottom fibres of the RC beam to experience tension. Once the applied load surpasses the tensile strength of the RC beam, the first crack forms. The load-deflection diagrams for all tested beams can be seen in Fig. 6. For CB1, the initial crack starts at load 45.07 kN, approximately the same as A1 45.10 kN, in which the crack typically initiates in the region where tensile stresses are highest, at the bottom of the middle section of the RC beams. This initial crack caused the stiffness of the structure to decrease, and deformation became more pronounced. CB1 records a deflection of 1.38 mm, while A1 shows a reduction of deformation to 0.59 mm, approximately 133% reduction of the deflection with the presence of steel strengthened. For the B1 beam, the initial crack of the beam occurs at load 75.00 kN, 67 % higher than beam CB1 and A1. The presence of the prestressing force of the Fe-SMA counteracts the tensile stress by inducing compressive forces before external loads are applied, delaying the initial crack occurrence. The deformation of B1 was recorded at 1.40 mm, approximately the same as CB1. In terms of deflection, beam A1 shows the lowest deflection among the beams.

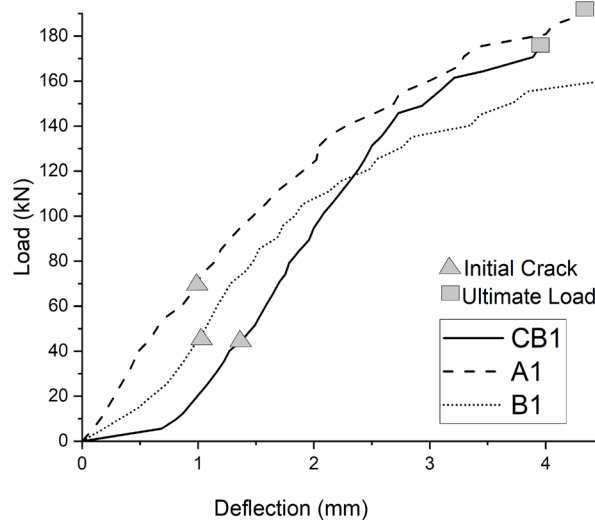


Fig. 6 Relationship of RC beams tested at room temperature

### 3.1.2 Elevated Temperature of 200°C

The load deflection for RC beam tested at elevated temperature of 200°C were presented in Fig. 7. For RC beams subjected to elevated temperature, CB2 records 12.5% reduction of initial crack load compared to CB1 which is at 40.20 kN and a deflection of 0.82 mm. For A2, the initial crack load is not affected by the elevated temperature, maintain the same initial crack load at 45.00 kN. However, the initial crack deformation was observed to increase to 0.93 mm. For B2, the initial crack load drops 25% compared to B1 at 60.59 kN, corresponding to a deflection of 0.78 mm. Although the RC beam was strengthened with steel or Fe-SMA, the initial crack point shows a reduction in the ductility of the beams. It is shown that elevated temperatures can have detrimental effects on the RC beams. At 200°C, compared to CB2, A2 performs 12.5% higher, while B2 performs significantly 50% higher in the initial crack load. The Fe-SMA-strengthened beam, B2, shows a 33% increase in the initial crack compared to steel strengthened beam, A2.

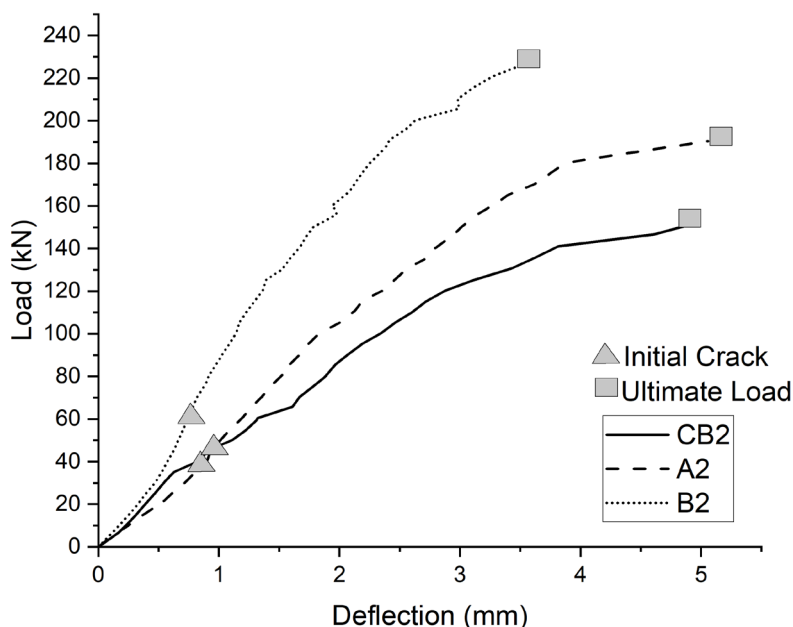


Fig. 7 Relationship of RC beams tested at elevated temperature of 200°C

## 3.2 Ultimate Load

### 3.2.1 Room Temperature

The experimental results shown in Fig. 6, revealed that the ultimate load of unstrengthen beam, CB1 is 175.19 kN with a deflection of 3.95 mm. Comparatively, specimen A1 strengthened with steel, exhibited a higher ultimate load of 202.24 kN, corresponding to a deflection of 5.50 mm, while RC beam strengthened with Fe-SMA, B1 had a lower ultimate load of 171.06 kN and a deflection of 4.99 mm. Upon analysing the data, it was discovered that Beam A1 demonstrated a significant difference with a higher ultimate load than Beam CB1 by approximately 15%, while 18% compared to A2. On the other hand, Beam B1, although having additional prestressing force, exhibited a lower ultimate load compared to beam CB1. This may be due to the beam's sudden failure, which caused the RC beam not to withstand higher tensile stress than A1. However, Beam A2 recorded higher deflection than the other two beams before reaching the ultimate load. The unexpected result, where Beam A1 exhibited a higher ultimate load than Beam B1, could be attributed to the incomplete activation of the Fe-SMA ribbed bar during the heating process using an oxy torch. Achieving the optimal activation temperature is crucial for harnessing the SME of Fe-SMA, contributing to its load-carrying capacity. However, using an oxy torch might result in non-uniform heating, leading to localised variations in temperature and preventing certain sections of the Fe-SMA ribbed bar from reaching the required activation temperature.

### 3.2.2 Elevated Temperature of 200°C

The Control Beam CB2 had the lowest ultimate load, at 150.72 kN at deflection of 4.88 mm, followed by Beam A2 with a 190.45 kN ultimate load corresponding to deflection of 5.06 mm and Beam B2 with a 225.91 kN ultimate load and 3.50 mm deflection as shown in Fig. 7. Beam A2 demonstrated a percentage difference of



approximately 26% higher ultimate load compared to CB2, while Beam B2 indicated a percentage difference of about 49% higher ultimate load. The strengthened RC beams, A2 and B2, demonstrate a significant enhancement of the load-bearing capacity of the RC beam at elevated temperatures, highlighting the advantages of these strengthening techniques. Moreover, the analysis results support the initial hypothesis that Beam B2, reinforced with Fe-SMA, had the highest ultimate load. Beam B2 had a higher ultimate load than Beams CB2 and A2 due to the prestressing effects of Fe-SMA, which most likely played a substantial influence in this. Elevated temperatures may have an effect on the Fe-SMA rebar's activation process. It is possible that during temperature exposure, the parts of the Fe-SMA that were initially anchored were protected from heat during the activation process and were subjected to heat during this process. This could result in uniform heating along the whole length of the Fe-SMA. This phenomenon is explained by the high temperature penetrating the concrete and evenly heating the Fe-SMA. B2 shows the highest load-bearing capacity even compared to A2, which is around 11% higher as a result of this event.

### 3.2.3 Effect of Temperature on Ultimate Load

There are intriguing differences between RC beams tested at ambient temperature and those tested at a higher temperature of 200°C when comparing the ultimate load findings. Specimens CB1, A1, and B1 at room temperature exhibited ultimate loads of 175.19 kN, 202.24 kN, and 171.06 kN, respectively, as presented in Table 5. However, when tested for an elevated temperature of 200°C, the ultimate loads recorded a significant difference. Due to degradation induced by the high temperature, specimen CB2 demonstrated a reduced ultimate load of 150.72 kN compared to Beam CB1. Note that Beam A2 measured an ultimate load of 190.45 kN, about 6% less than Beam A1 in terms of percentage differences, most likely due to the high-temperature exposure. Interestingly, for Beam B2, the ultimate load obtained was 225.91 kN, which suggested an increment of 32% compared to Beam B1 (specimen at room temperature). As previously explained, the attribute of the non-uniform heating of the Fe-SMA ribbed bar during the activation process, which resulted in the partial prestressing effects by the Fe-SMA in the concrete, made it possible for Beam B1 to have a reduced ultimate load. However, as expected, Beam B2 revealed the highest ultimate load under 200°C circumstances. Note that the higher temperature probably made the Fe-SMA ribbed bar's activation more uniform and thorough, effectively harnessing its prestressing characteristic and significantly increasing beam B2's load-carrying capacity. Additionally, the NSM processes' preset anchoring lengths at both ends were inactive. However, during the high-temperature exposure, these inactive lengths immediately became active, helping to strengthen the beam further. It can be concluded that at 200°C, the prestressing losses of Fe-SMA do not occur, and beam B2 performs even better than the RC beam strengthened with steel.

**Table 5** Summary results of the tested RC beams

Beam ID	Room Temperature			200°C		
	CB1	A1	B1	CB2	A2	B2
Initial Crack (kN)	45.07	45.10	75.00	40.20	45.00	60.59
Mid-span Deflection at Initial Crack (mm)	1.38	0.59	1.40	0.82	0.93	0.78
Ultimate Load (kN)	175.19	202.24	171.06	150.72	190.45	225.91
Mid-span Deflection at Ultimate (mm)	3.95	5.50	4.99	4.88	5.06	3.50

## 3.3 Load-Strain Behaviour

### 3.3.1 Room Temperature

The load versus tensile strain graph for the RC beam at room temperature is illustrated in Fig. 8. When RC beams are subjected to external load, the RC beam undergoes strain deformation. Strain is a measure of the amount of deformation relative to the original dimensions of the beam. The load strain results show the RC beams' deformation at the tension area. The experimental strain deformation values for both sides were similar, and only one strain measurement was reported in this study. CB1 and A1 beams exhibited a similar trend of the load-strain relationship, indicating that both beams had a similar behaviour. A similar behaviour is because beam A1 was strengthened using the same steel properties as beam CB1. The NSM steel strengthening provides additional strength as the steel reinforcement ratio increases without additional forces, unlike beam A1, which provides additional prestressing forces. Before the initial crack load occurs, CB1 and A1 RC beams behave elastically. The linear trends of the load-strain relationship indicated this elastic behaviour, which aligned with the load-deflection curve until the first cracks in the beams were occurrence.

Upon reaching their initial crack load, 42.5 kN and 44.36 kN, for CB1 and A1, the curve shows a non-linear relationship beyond this point. This value is approximately the same as from the observation of the initial crack at 45 kN for both CB1 and A1. The strain for CB1 and A1 are recorded at 61  $\mu\text{m}$  while A1 increases up to 100  $\mu\text{m}$ . In beam B1, the increase in the initial crack load significantly influences the strain of the beam. The strain gage records the highest strain reading at 212  $\mu\text{m}$  corresponding to 75.15 kN before the initial crack occurrence, which is similar to the observed initial crack. All tested RC beam strain measurements were obtained only during the initial crack load due to severe deformation beyond the initial crack. This deformation was caused by the crack propagation run through the installed strain gages, making the strain gage reading unreliable.

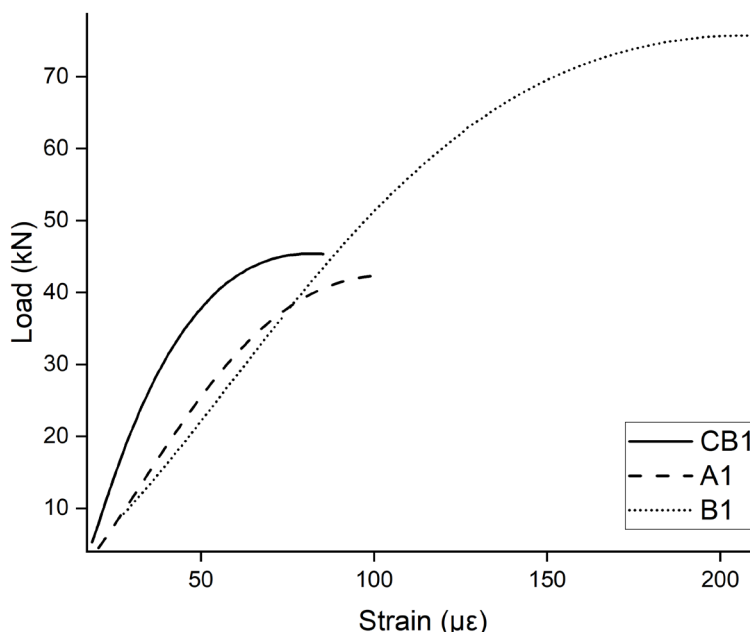


**Fig. 8** Load versus strain of RC beam tested at room temperature

### 3.3.2 Elevated Temperature of 200°C

For RC tested at elevated temperatures, the strain measurement shows an increased trend of strain measurement for all tested beams while having a reduction of initial crack load, as depicted in Fig. 9. When RC beams were exposed to 200°C, the temperature caused mild thermal stress, which prompted the loss of bound water and the start of decomposition of calcium-silicate hydrate (C-S-H), resulting in the weakening of the binder between the cement and concrete. The initial crack that caused the strain deformation in CB2 was observed at 39.43 kN, close to the observed first initial crack at 40 kN, corresponding to a strain measurement of 299  $\mu\text{m}$ . A2 has a slightly higher value than the observed initial crack and from the load-strain deflection relationship. The observed initial crack happens at 45 kN, while the initial crack determined from the load-strain curve is at 35.31 kN, corresponding to a strain measurement of 329  $\mu\text{m}$ , lower than the observations. The disparity between visual observation and strain measurement can be attributed to the sensitivity and precision of each method. Strain gages are highly sensitive and can detect even minute deformation in the concrete. It can pick up strains occurring within the concrete, including microcracks. Subjectively, for visual observation, the determination of the initial crack relies on the human eye, which may not detect microcracks or hairline fractures that occur at the early stages. Even at elevated temperatures, the load-strain relationship of beam CB2 and beam A2 show similar trends as those highlighted previously at room temperature. For B2, the initial crack load corresponding to the load-strain relationship is about 59.76 kN at strain of 189  $\mu\text{m}$ , approximately the same as observed at 60 kN. By covering the Fe-SMA with the NSM technique, the elevated temperatures do not significantly harm the prestressing forces, which helps the beam B2 sustain its performance. Compared to steel strengthening, Fe-SMA strengthening shows higher performance in reducing the strain of the RC beams. The preference for lower or higher strain in structure depends on various factors. Excessive strain deformation can affect the serviceability of a structure. In the context of strengthening RC beams, deformation is a crucial factor, making it preferable to aim for reduced strain.

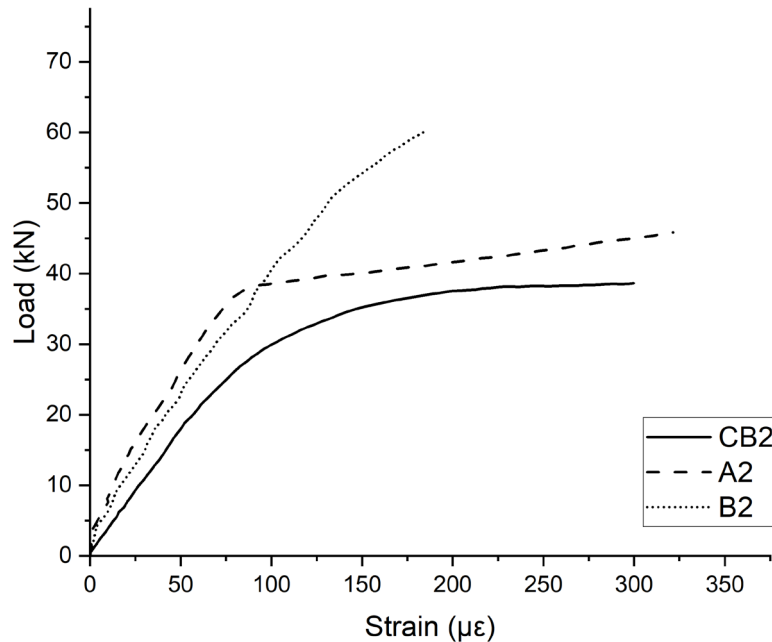


Fig. 9 Load versus strain of RC beam tested at elevated temperature of 200°C

### 3.3.3 Effect of Elevated Temperature on Strain

The elevated temperature influences the RC beam's strain deformation and reduces the initial crack. All RC beams exposed at elevated temperatures had higher strain than room temperature. This RC beam experiences higher elongations in response to elevated temperatures of 200°C. For the unstrengthened RC beam, CB2 shows three times more strain deformation than CB1. This indicates that the RC beam loses its stiffness and strength when exposed to elevated temperatures. For RC beams strengthened with steel, the strain difference between A2 and A1 shows that A2 doubles the strain elongation of A1. Although the initial crack load is similar, the difference between the strains shows that the steel-strengthened beam had to withstand additional strain deformation in order to withstand the same initial crack. For beam B2, the Fe-SMA strengthened RC and lost its initial crack due to elevated temperatures, which is the same as other beams; however, the strain deformation is lower by about 10% compared to B1. The Fe-SMA strengthening proved that although at elevated temperatures, strengthening the RC beam using Fe-SMA is a better solution in controlling the stiffness of the beams, and Fe-SMA does not compromise the load-bearing capacity of the beam. Additionally, Fe-SMA prestressing forces do not significantly lose their prestressing force at this elevated temperature.

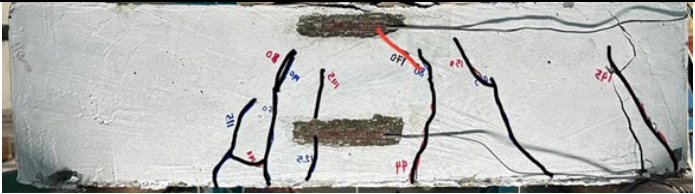
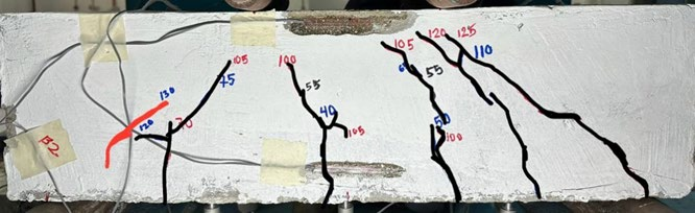
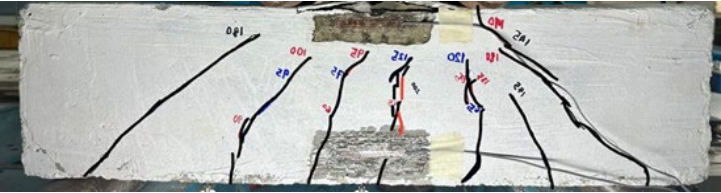
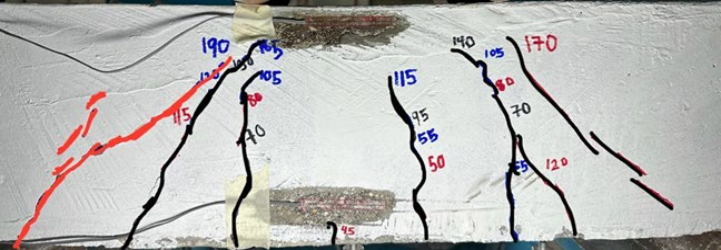
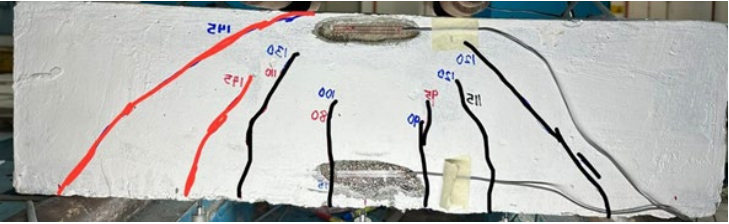
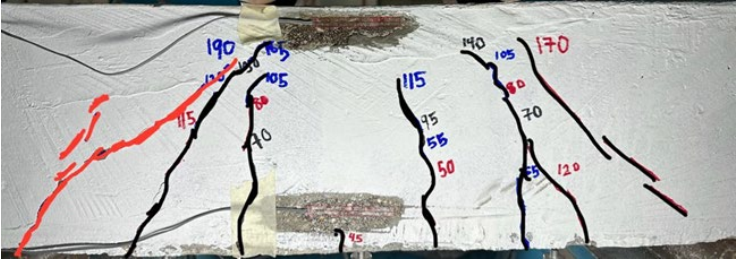
### 3.4 Crack Propagation

When a beam fails, crack patterns can reveal information about the failure mode. The loads and forces exerted on the beam from the outside impact these crack patterns. The tensile zone at the bottom of the beam is where cracks usually originate in a standard RC beam. Additionally, these cracks begin and spread as the strain on the beam rises, indicating the buildup of tension within the concrete. The crack propagation were observed during the testing of the RC beams and were recorded. Table 6 displays the crack propagations of the RC beams.

At room temperature, the unstrengthened beam, CB1 and Beam A1, strengthened with steel exhibited first crack initiation when the load was recorded at 45 kN, indicating that the steel bar may not have had a major impact on the initial crack formation. Nevertheless, with the same initial crack loads, A1 beam crack propagation are more well distributed compared to CB1 until its ultimate load. For Beam B1, the initial crack developed at a higher load of 75 kN due to the special characteristics of Fe-SMA ribbed bars, which enable them to display increased compressive stress capacity and counteracts the tensile stress caused by the applied load, improving the initial crack development. This result reflects similar observation in Shahverdi et al. [29], who demonstrated that activating Fe-SMA for RC beam strengthening helped to increase the initial crack load, compared to passive strengthening materials such as FRP. The crack initiation behaviour of the RC beams had unique responses at a higher temperature of 200°C. At a reduced load of 40 kN, Beam CB2 developed the first crack, demonstrating the reduction in concrete strength brought on by the high temperatures. Furthermore, Beam A2 indicated a slightly greater load at first fracture when reinforced with a steel ribbed bar, with the crack initiation occurring at 45 kN. Despite the adverse impacts of increased temperature on concrete strength, the presence of the steel ribbed bar likely provided some barrier to crack development. Notably, at 60 kN, Beam B2 demonstrated delayed crack

onset. These results suggest the divergent influences of various strengthening materials on the fracture initiation behaviour of RC beams at various temperatures. At higher temperatures, Fe-SMA ribbed bars demonstrated greater crack resistance and delayed crack onset, whereas steel bars indicated no effect.

**Table 6** Crack propagation of RC beams

Beam ID	Failure Load (kN)	Crack Propagation
CB1	175.16	
CB2	150.72	
A1	202.25	
A2	190.45	
B1	171.06	
B2	225.91	

### 3.5 Conclusions

This study proved that it is possible and does not advocate for complicated methods to apply NSM technology to strengthen the RC beam while improving beam performance. In conclusion, there were substantial differences in the load-carrying capacity of the RC beams evaluated at room temperature and an elevated temperature of 200°C, based on the comparison of ultimate load data. At room temperature, Beams CB1, A1, and B1 displayed ultimate loads of 175.19 kN, 202.25 kN, and 171.06 kN, respectively. However, when subjected to a temperature of 200°C, the ultimate loads changed notably. Beam CB2 exhibited the lowest ultimate load of 150.72 kN, representing a reduction of 16% compared to its counterpart, Beam CB1. Meanwhile, Beam A2 recorded an ultimate load of 190.45 kN, indicating a percentage difference of approximately 6% lower as compared to Beam A1 at room temperature. Most notably, Beam B2 displayed an ultimate load of 225.91 kN, representing an impressive 32% increment compared to Beam B1. The observed lower ultimate load for Beam B1 at room temperature was probably attributed to the non-uniform heating of the Fe-SMA ribbed bar during the activation process, resulting in an incomplete prestressing effect. Nevertheless, Beam B2 exhibited the highest ultimate load, indicating that the elevated temperature facilitated a more uniform and complete activation of the Fe-SMA ribbed bar, effectively harnessing its prestressing behaviour and significantly enhancing Beam B2's load-carrying capacity. The elevated temperature not only significantly affects the load-bearing capacities but also the RC beam's deformation. Results of the load-strain relationship show that the unstrengthened RC beam experienced significant strain deformation at the initial crack load at elevated temperature conditions. In contrast, RC beam strengthened with steel manage to sustain the same initial crack load but experience higher strain deformation. Fe-SMA strengthened beams, and although the elevated temperature of 200°C reduced the initial crack load, the Fe-SMA managed to sustain the strain deformation during the initial crack. The beam's strengthening material helps to disperse the crack more uniformly. By limiting the development of large, uncontrollable cracks, evenly distributed cracks increase the beam's durability. The study's findings highlight the potential of NSM strengthening technology in RC structures. Hence, the choice of materials used in the strengthening procedures may provide a significant result in the performance of the final strengthened element. For instance, in this study, the Fe-SMA ribbed bar maintains its strength and enhances the resilience of RC beams even in elevated temperature environments. The results demonstrated that Fe-SMA ribbed bar strengthening does not suffer from a loss of strength at high temperatures compared to conventional steel ribbed bars in the NSM strengthening.

### Acknowledgement

This study was funded by the Ministry of Higher Education Malaysia under Fundamental Research Grant Scheme (FRGS/1/2021/TK0/UITM/02/41). The authors would also like to thank Universiti Teknologi MARA, Cawangan Pulau Pinang, for all the support.

### Conflict of Interest

Authors declare that there is no conflict of interests regarding the publication of the paper.

### Author Contribution

*The authors confirm contribution to the paper as follows: **study conception and design:** Muhammad Adam Syahmi Dazulhisham, Muhammad Arif Ikmal Abdul Halim, Lyn Dee Goh; **data collection:** Muhammad Adam Syahmi Dazulhisham, Muhammad Arif Ikmal Abdul Halim; **analysis and interpretation of results:** Muhammad Adam Syahmi Dazulhisham, Muhammad Arif Ikmal Abdul Halim, Lyn Dee Goh; **draft manuscript preparation:** Muhammad Adam Syahmi Dazulhisham, Muhammad Arif Ikmal Abdul Halim, Lyn Dee Goh. All authors reviewed the results and approved the final version of the manuscript.*

### References

- [1] Attia, M. M., Abdelsalam, B. A., Tobbala, D. E., & Rageh, B. O. (2023) Flexural behavior of strengthened concrete beams with multiple retrofitting systems, *Case Studies in Construction Materials*, 18, e01862, <https://doi.org/10.1016/j.cscm.2023.e01862>
- [2] Qiang, X., Wu, Y., Wang, Y., & Jiang, X. (2023) Research Progress and Applications of Fe-Mn-Si-Based Shape Memory Alloys on Reinforcing Steel and Concrete Bridges, *Applied Sciences*, 13(6), 3404, <https://doi.org/10.3390/app13063404>
- [3] Siddika, A., Al Mamun, M. A., Ferdous, W., & Alyousef, R. (2020) Performances, challenges and opportunities in strengthening reinforced concrete structures by using FRPs—A state-of-the-art review, *Engineering Failure Analysis*, 111, 104480, <https://doi.org/10.1016/j.engfailanal.2020.104480>

- [4] Abdalla, J. A., Abu-Obeidah, A. R., & Hawileh, R. A. (2019) Use of aluminum alloy plates as externally bonded shear reinforcement for R/C beams, *Procedia Structural Integrity*, 17, 403-410, <https://doi.org/10.1016/j.prostr.2019.08.053>
- [5] Chalioris, C. E., & Pourzitidis, C. N. (2012) Rehabilitation of shear-damaged reinforced concrete beams using self-compacting concrete jacketing, *International Scholarly Research Notices*, 2012, <https://doi.org/10.5402/2012/816107>
- [6] Chin, C. L., Ma, C. K., Tan, J. Y., Ong, C. B., Awang, A. Z., & Omar, W. (2019) Review on development of external steel-confined concrete, *Construction and Building Materials*, 211, 919-931, <https://doi.org/10.1016/j.conbuildmat.2019.03.295>
- [7] Li, C., & Aoude, H. (2023) Effect of UHPC jacketing on the shear and flexural behaviour of high-strength concrete beams, *Structures*, 51, 1972-1996, <https://doi.org/10.1016/j.istruc.2023.03.104>
- [8] Wang, H. T., Bian, Z. N., Chen, M. S., Hu, L., & Wu, Q. (2023) Flexural strengthening of damaged steel beams with prestressed CFRP plates using a novel prestressing system, *Engineering Structures*, 284, 115953, <https://doi.org/10.1016/j.engstruct.2023.115953>
- [9] Siddika, A., Al Mamun, M. A., Alyousef, R., & Amran, Y. M. (2019) Strengthening of reinforced concrete beams by using fiber-reinforced polymer composites: A review, *Journal of Building Engineering*, 25, 100798, <https://doi.org/10.1016/j.jobe.2019.100798>
- [10] Su, M., Gong, S., Liu, Y., & Peng, H. (2022) Flexural behavior of RC beams strengthened with fully or partially prestressed near-surface mounted FRP strips: An experimental investigation, *Engineering Structures*, 262, 114345, <https://doi.org/10.1016/j.engstruct.2022.114345>
- [11] ACI Committee 440, & American Concrete Institute. (2017) Guide for the design and construction of externally bonded FRP systems for strengthening concrete structures. American Concrete Institute.
- [12] Sanginabadi, K., Yazdani, A., Mostofinejad, D., & Czaderski, C. (2022) RC members externally strengthened with FRP composites by grooving methods including EBROG and EBRIG: A state-of-the-art review, *Construction and Building Materials*, 324, 126662, <https://doi.org/10.1016/j.conbuildmat.2022.126662>
- Mahmoud, K. M., Sallam, E. A., & Ibrahim, H. M. H. (2022), Behavior of partially strengthened reinforced concrete columns from two or three sides of the perimeter, *Case Studies in Construction Materials*, 17, e01180, <https://doi.org/10.1016/j.cscm.2022.e01180>
- [13] Karim, S. H., & Karim, F. R. (2020) Review on the Strengthening of Reinforced Concrete Columns by Reinforced Concrete Jacketing, *Saudi Journal of Civil Engineering*, <https://doi.org/10.36348/sjce.2020.v04i01.002>
- [14] De Lorenzis, L., & Teng, J. G. (2007) Near-surface mounted FRP reinforcement: An emerging technique for strengthening structures, *Composites Part B: Engineering*, 38(2), 119-143, <https://doi.org/10.1016/j.compositesb.2006.08.003>
- Xing, G., Ozbulut, O. E., Al-Dhabyani, M. A., Chang, Z., & Daghash, S. M. (2020) Enhancing flexural capacity of RC columns through near surface mounted SMA and CFRP bars, *Journal of Composite Materials*, 54(29), 4661-4676, <https://doi.org/10.1177/0021998320937054>
- Zhang, S. S., Yu, T., & Chen, G. M. (2017) Reinforced concrete beams strengthened in flexure with near-surface mounted (NSM) CFRP strips: Current status and research needs, *Composites Part B: Engineering*, 131, 30-42, <https://doi.org/10.1016/j.compositesb.2017.07.072>
- Geetha, S., & Selvakumar, M. (2021) Self prestressing concrete composite with shape memory alloy, *Materials Today: Proceedings*, 46, 5145-5147, <https://doi.org/10.1016/j.matpr.2020.10.677>
- [15] Hong, K. N., Yeon, Y. M., Ji, S. W., & Lee, S. (2022) Flexural behavior of RC beams using Fe-based shape memory alloy rebars as tensile reinforcement. *Buildings*, 12(2), 190, <https://doi.org/10.3390/buildings12020190>
- [16] Obaydullah, M., Jumaat, M. Z., Alengaram, U. J., ud Darain, K. M., Huda, M. N., & Hosen, M. A. (2016). Prestressing of NSM steel strands to enhance the structural performance of prestressed concrete beams, *Construction and Building Materials*, 129, 289-301, <https://doi.org/10.1016/j.conbuildmat.2016.10.077>
- [17] Cladera, A., Weber, B., Leinenbach, C., Czaderski, C., Shahverdi, M., & Motavalli, M. (2014) Iron-based shape memory alloys for civil engineering structures: An overview, *Construction and Building Materials*, 63, 281-293, <https://doi.org/10.1016/j.conbuildmat.2014.04.032>
- [18] Hasnat, A., Ahmed, S. T., & Ahmed, H. (2020) A review of utilising shape memory alloy in structural safety. *AIUB Journal of Science and Engineering (AJSE)*, 19(3), 116-125, <https://doi.org/10.53799/ajse.v19i3.111>
- [19] El-Hacha, R., & Rojob, H. (2018) Flexural strengthening of large-scale reinforced concrete beams using near-surface-mounted self-prestressed iron-based shape-memory alloy strips. *PCIJ*, 63(6), 51-62, <https://doi.org/10.15554/pcij63.6-03>

- [20] Michels, J., Shahverdi, M., & Czaderski, C. (2018) Flexural strengthening of structural concrete with iron-based shape memory alloy strips, *Structural Concrete*, 19(3), 876-891, <https://doi.org/10.1002/suco.201700120>
- [21] Rojob, H., & El-Hacha, R. (2018) Performance of RC beams strengthened with self-prestressed Fe-SMA bars exposed to freeze-thaw cycles and sustained load, *Engineering Structures*, 169, 107-118, <https://doi.org/10.1016/j.engstruct.2018.04.009>
- [22] Czaderski, C., Shahverdi, M., Ghafoori, E., Motavalli, M., Leinenbach, C., Arabi-Hashemi, A., ... & Scherer, J. (2019, August). The development of memory steel at Empa. In *5th International Conference on Smart Monitoring, Assessment and Rehabilitation of Civil Structures (SMAR)*, Potsdam, Germany. <https://www.ndt.net/?id=24938>
- [23] Shahverdi, M., Christoph, C., Annen, P., Motavalli, M. (2016) Strengthening of RC beams by iron-based shape memory alloy bars embedded in a shotcrete layer. *Engineering Structures*, 117, 263-273, <https://doi.org/10.1016/j.engstruct.2016.03.023>  
Zhang, Z.-X., Zhang, J., Wu, H., Ji, Y., & Kumar, D. D. (2022) Iron-Based Shape Memory Alloys in Construction: Research, Applications and Opportunities, *Materials*, 15(5), 1723, <https://doi.org/10.3390/ma15051723>
- [24] Shahverdi, M., Czaderski, C., & Motavalli, M. (2016) Iron-based shape memory alloys for prestressed near-surface mounted strengthening of reinforced concrete beams, *Construction and Building Materials*, 112, 28-38, <https://doi.org/10.1016/j.conbuildmat.2016.02.174>